FUDMA Journal of Sciences (FJS)
ISSN online: 2616-1370
ISSN print: 2645 - 2944
Vol. 3 No. 3, September, 2019, pp 58 –75

RADIOMETRIC NORMALIZATION OF ASTER, LANDSAT TM AND ETM+ SENSORS FOR MULTI-TEMPORAL NORMALISED DIFFERENCE VEGETATION INDEX DATA QUALITY IN A DRYLAND WOODLAND RESERVE.

[1,2*]Badamasi, M. M.

[1]Department of Environmental Management, Bayero University Kano
[2]Centre for Dryland Agriculture, Bayero University Kano

Corresponding authors email: mmbadamasi@gmail.com

ABSTRACT
Images acquired at different times and from different sensors for multi-temporal assessment usually have different amounts of haze and dust in the atmosphere. These differences can mask real changes or make similar land cover appears to have changed. Thus, the use NDVI for multi-temporal assessment derived from multi-sensor satellite images require radiometric normalization. In this study, Landsat TM, ETM+ and ASTER products were used. Empirical scene normalization technique was used balancing the radiometric attributes of the products after geometric rectification and atmospheric correction. The results showed that empirical normalization via PIFs have significance positive influence on the quality of NDVI and it is capable further reducing noise in the image.

Keywords: Radiometric normalization, PIFs, NDVI, Drylands

INTRODUCTION

Vegetation has been identified as an important indicator for monitoring changes in the climate-human-natural environment. Studies on vegetation changes within the African landscape especially the savanna has shown large scale pressure owing to deforestation in the last three decades. These disturbances may threaten vegetation carbon stock, ecosystem services and global change (Brandt *et al*, 2018). Remote sensing has been very handy in handling issues relating to vegetation change, especially with the use of optical sensors due to their repetitive coverage at a short time interval (Rustamov *et al*., 2012; Syariz *et al*., 2019). The hypothetic radiometric stability of satellite sensors is the main essence for remote sensing applications using multi-temporal satellite images, and the radiometric consistency of the acquired images (Syariz *et al*., 2019). However, a problem associated with using historical remotely sensed data for change detection is that the data are usually from non-anniversary dates with varying sun angle, atmospheric, and soil moisture conditions (Paolini *et al.*, 2006) and sometimes from different sensors. The multiple dates of remotely sensed data should be normalized so that these effects can be minimized or eliminated (Syariz *et al*., 2019).

A number of approaches to radiometric normalization are presented in the literature. These include the use of anniversary dates (Lambin, 1996), histogram matching (Prakash and Gupta, 1998), dark area subtraction (Vincent, 1972), improved dark area subtraction (Chavez, 1988), radiance to reflectance conversion using known targets (Campbell, 1996), atmospheric modeling (Kneizys *et al.*, 1988) and linear transformation based on reflectance-invariant objects (Heo and Fitzhugh, 2000, McGovern *et al.*, 2002, Du, *et al.*, 2002). No single approach has universal application because solutions are location, application and image dependent. Analysts must, therefore, be aware of existing procedures and be prepared to use or adapt these, or develop alternative procedures, as appropriate (McGovern, *et al.*, 2002). This study utilizes the indirect empirical scene normalization technique because all the parameters necessary for computing it were available.

The empirical scene normalization approach (Jensen, *et al.*, 1995) attempts to make equivalent spectral bands (from the different dates) appear as though imaged through the same sensor, under similar illumination conditions and the same atmosphere for each image (Munyati, 2000). It involves selecting a base image (b) and then transforming the spectral characteristics of all other images obtained on dates *b*-1, *b*-2, and/or *b*+1, *b*+2, etc. To have approximately the same radiometric scale as the base image (Jensen, 2005). It is important to remember, however, that the radiometric scale used in a relative multiple-date image normalization will most likely be simple brightness values (e.g. *BV* with range from 0-255). Hence, DN values were used in this study. The procedure involves the selection of pseudo-invariant features (PIFs), referred to as radiometric ground control points. These are ground targets common to the images, which are considered to be constant reflectors over time. Constant reflectors hardly exist, hence the concept of false (pseudo) features whose reflectance is relatively constant with the background assumption that their reflectance is constant. For these PIFs any change in their

brightness values (*BV*) on the multi-temporal image set will be attributed to detector calibration, astronomic, atmospheric and phase angle differences. The targets used need not be the same throughout the multi-temporal image set (Hall, *et al.,* 1991, Du et al., 2002; Zhang, et al., 2014). Once the targets have been chosen, their brightness values on the respective bands are regressed against their corresponding values on the equivalent bands. In the resulting regression model, the additive component corrects for the difference in atmospheric path radiance between dates, and the multiplicative terms corrects for the difference in detector calibration, sun angle, earth/sun distance, atmospheric attenuation and phase angle between dates (Jensen, *et al.*, 1995). After the removal of these variations, changes in brightness value could be related to changes in surface conditions. Recently, Zhou et al. (2016) presented the utilization of normalized difference water index (NDWI) to select initial PIFs, and several statistical rules are adopted to select final PIFs. According to Eckhardt, *et al.* (1990) the potential PIFs for radiometric normalization should have the following characteristics for them to be of value in a multiple date image normalization process:

1. The spectral characteristics of the PIFs should change very little through time, although it is acknowledged that some change is inevitable. Deep non-turbid water bodies, bare soil, large rooftops, or other homogeneous features are candidates.
2. The PIFs should be at approximately the same elevation as the other land in the scene. Selecting a mountaintop PIF would be of little use in estimating atmospheric condition near sea level because most aerosols in the atmosphere occur within the lowest 1000m.
3. The PIF should normally contain only minimal amount s of vegetation. Vegetation spectral reflectance can change over time as a result of environmental stress and plant phenology. However, an extremely stable, homogeneous forest canopy imaged on near anniversary dates might be considered.
4. The PIF must be in a relatively flat area so that incremental changes in sun angle from date to date will have the same proportional increase or decrease in direct beam sunlight for all normalization targets.

This study examined the influence of multi-sensor and multi-temporal satellite image radiometric normalization on the quality of normalised differential vegetation index (NDVI) using a woodland reserve as a case study site to test the effectiveness of the technique for sustained monitoring of vegetation as an important global change indicator.

Data

Study Area

Falgore Game Reserve (FGR), formerly Kogin Kano Forest Reserve is woodland forest located on longitudes 8º 30' to 8º 50' East and latitudes 10º 46' to 11º 20' North, some 110 km south of Kano on the Jos-Kano road (Figure 1). It has an aerial extent of 92,000 ha. The northern boundary is formed by the artificial Lake Tiga which, when full, submerges the north-western tip of the reserve. To the south-east of Falgore lies Lame Burra Game Reserve (205,900 ha) in Bauchi State (BirdLife International, 2007).

The present climate of the FGR is tropical wet-and –dry type, coded *Aw* by W. Koppen (Kottek *et. al*., 2006), mean annual rainfall is estimated at 1000mm and this value decreases northward (Liman *et. al*., 2014). The mean annual temperature is about 24ºC, but the mean monthly values range between 21ºC in the coolest months (December/ January) and 31ºC in the hottest months (April/May) (Liman *et. al*, 2014). The elevation of their bases ranges between 700m and 800m. The highest peak is about 1230m above sea level. The FGR has a high density tree species and high floristic variations found within the open Northern Guinea Savanna woodland vegetation type, though with elements of the Sudan Savanna in the northern tip (Badamasi, 2014). Example includes*Isoberliniadoka, Khayasenegalensis, Vitexdoniana, Anogeissusleiocarpus, Tamarindusindica, Detariummicrocarpum and Pterocarpuserinaceus* (BirdLife International, 2007).

Data

Landsat Thematic Mapper (TM), Enhanced Thematic Mapper Plus (ETM+) and Advanced Space-borne Thermal Emission and Reflection Radiometer (ASTER) image (Table 1) were used in evaluating the radiometric normalization method. For simplicity only bands 3 and 4 on board the Landsat series and bands 2 and 3 of the ASTER image corresponding to the red and near infra-red band respectively were extracted for this study.

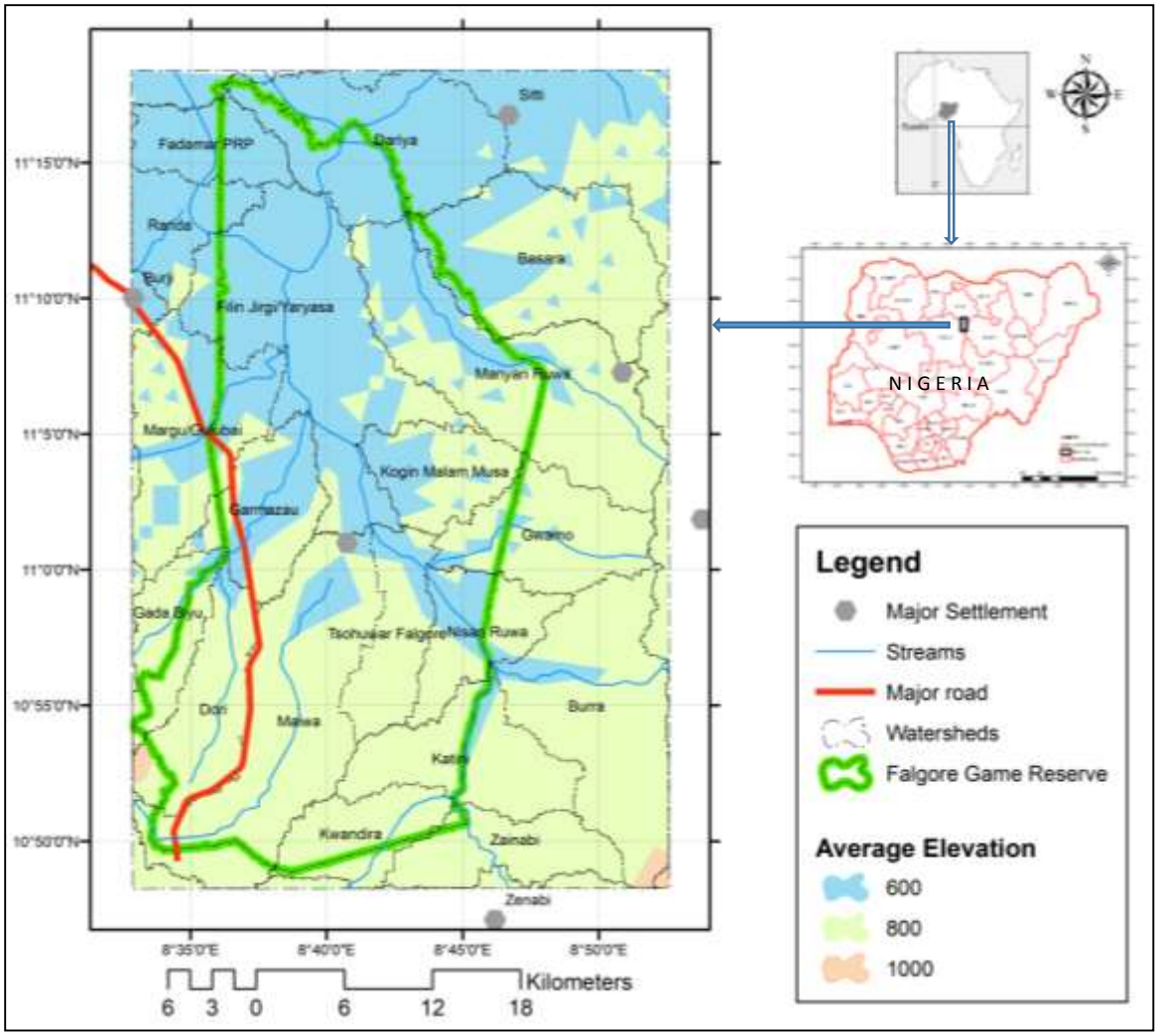

Fig. 1. Falgore Game Reserve

Table 1: Landsat and ASTER data used

Images Used for the study	Path/row	Resolution	Date of acquisition	Format	Product Type (Cloud Cover %)
Landsat 5 TM[a] Band 1 -7	188/052	30m	19-12-1986	GEOTIFF	L1T (0%)
Landsat 4 TM[a] Band 1 -7	188/052	30m	22-12-1990	GEOTIFF	L1T (0%)
Landsat 5 TM[a] Band 1 -7	188/052	30m	18-11-1998	GEOTIFF	L1T (0%)
Landsat 7 ETM+[a] Band 1 -8	188/052	30	17-12-2000	GEOTIFF	L1T (0%)
ASTER Band 1-14[b]		15m	29-11-2005	HDF	AST_L1B (0%)

Note: TM = thematic mapper; ETM+ = enhanced thematic mapper plus; ASTER = Advanced Spaceborne Thermal Emission and Reflection Radiometer

Source: [a]Free from *http://glovis.usgs.gov*;[b]Purchased from *http://glovis.usgs.gov*,

Near anniversary images have been suggested to reduce error arising from seasonal differences (vegetation phenology cycles) when undertaking change detection analyses (Jensen, 2000; Munyati, 2000; Lillesand *et al.,* 2004). Although Abubakar (1998) suggested the month of May (first week) as a suitable period for inclusion in change detection analysis in Sudano-Sahelian zone, considering the period as having few rain drops making permanent vegetation cover to have established and crops at this stage have not developed. Accordingly, much of the green reflectance from the surface is due to permanent vegetation. The problem with such criteria is that the onset of rainfall usually fluctuates and this might have introduced some noise in form of cloud cover to the image acquired on such date. In addition, ground truthing exercise which is usually conducted in almost near anniversary with the referenced image might create mixed up in terms of classification of spectral signature recognition. Hence, the research utilized an alternative month that is quite stable and free of the aforementioned short comings. November and December images (winter period in the study area) were chosen for a number of reasons. At this time of the year, rainfall has seized for few months or weeks and other cropland at this time have been harvested leaving trees still with green leaves. Irrigated areas are yet or about planting their crops. This minimizes the conflict in the spectral signatures of green trees that may confuse the greenness level for crops during the rainy season. Although trees in this area are deciduous in nature, but the high soil moisture content still sustains the greenness of the leaves. In addition dry season images are largely cloud-free. Finally only November/December images were found to be consistent in terms of their availability in the archives for both ASTER and Landsat data series. Vegetation Index including NDVI used for this study is often considered as supervised enhancement technique (Liu and Mason, 2009) which have the capability of highlighting the *red edge* (the significant difference between red and NIR) for projecting vegetation spectra among other spectral features, and suppresses the effects of topography and shade (Jensen, 2005). NDVI is well known to correlate with vegetation biomass and net primary production. This has therefore paved way for using NDVI for the current study.

Data pre-processing

Images acquired at different times usually have different amounts of haze and dust in the atmosphere. This is because the radiance recorded at the sensor is a function of surface condition, sun angle, earth-sun distance, detector calibration, atmospheric condition and sun-target-sensor geometry (Jensen, 1996). These differences can mask real changes or make similar land cover appears to have changed. Since the multi-temporal image dataset used was acquired with different sensor, sun angles and most likely different atmospheric composition, they had different illumination condition. To overcome this problem the images must be geometrically rectified to a common map projection and ideally they should be radiometrically normalized to remove the effects of non-surface related difference in recorded radiance.

Atmospheric correction

To correct for atmospheric attenuation in the images the Cost model developed by Chavez (1996) was applied to all bands 3 and 4 of the Landsat series and bands 2 and 3 of the ASTER image. The ASTER image was later use as the reference image. The Cost model incorporates all of the elements of the Dark Object Subtraction model (for haze removal) plus a procedure for estimating the effects of absorption by atmospheric gases and Rayleigh scattering. It requires no additional parameters over the Dark Object Subtraction model and estimates these additional elements based on the cosine of the solar zenith angle (90 – solar elevation).

With the Cost model, the down-welling spectral irradiance is assumed to be 0.0. However, the atmospheric transmittance is estimated as the cosine of the solar zenith angle (90 – solar elevation), and path radiance due to haze is estimated by specifying the DN of objects that should have a reflectance of zero (e.g., deep clear lakes). Spectral diffuse sky irradiance is also assumed to be 0.0. The spectral solar irradiance was then calculated automatically: based on the wavelength specified, a value of mean spectral solar irradiance was interpolated from values in a look up table taken from Thekaekara *et al.* (1969), which is then adjusted for annual variations by multiplying the interpolated value developed by Cracknell and Hayes (1991). The units calculated are in $mWcm^{-2}sr^{-1}um^{-1}$. The parameters used for the Cost model were extracted from the respective image Metadata files that accompanied the Landsat image series (1986, 1990, 1998, and 2000) as well as the ASTER image of 2005, summarized in Table 2. This was then implemented using the Image Restoration Module (ATMOSC-atmospheric correction) in Idrisi Taiga.

This procedure was used to correct bands 3 and 4 of the whole Landsat TM and ETM+, and bands 2 and 3 of the Aster imageries which were later used in deriving NDVI images. Most studies have shown that failure to correct for atmospheric effects influences classification results and NDVI values (Kaufman, 1989). The process produced a reflectance value for all the images. Furthermore, the Cost model is known to remove haze and correct for the effect of atmospheric gases and Rayleigh scattering (Berberoglu and Akin, 2009).

Table 2: Parameters used for implementing COST model

Year	Sun elevation	Satellite viewing angle (90^o – Satellite angle at near nadir)	Time (GMT)	Band	Wavelength of band center (microns)	Lmin	Lmax	DN haze^
1986	41.8871600	8.2	14.03527	2- G	0.56325	-0.284	33.30	44
				3- R	0.66	-1.17	26.40	39
				4- NIR	0.825	-1.51	22.10	**15**
1990	41.9485738	8.2	14.13593	2- G	0.56325	-2.84	33.60	**3**
				3- R	0.66	-1.17	25.40	4
				4- NIR	0.825	-1.51	22.10	17
1998	49.4725366	8.2	14.37061	2- G	0.56325	-2.84	36.50	22
				3- R	0.66	-1.17	26.40	19
				4- NIR	0.825	-1.51	22.10	**10**
2000	46.3704704	8.2	14.56031	2- G	0.56325	-6.4	19.65	44
				3- R	0.66	-5.0	15.29	39
				4- NIR	0.825	-5.1	24.11	**15**
2005	52.6019760	0.019	14.99700	1- G	0.556	0*	1*	Nil
				2- R	0.661	0*	1*	Nil
				3N- NIR	0.807	0*	1*	Nil

^ = this is path radiance due to haze and it is estimated by specifying the DN of objects that should have a reflectance of zero (e.g., deep clear lakes) as such DN minimum is usually specified to account for Dark object subtraction (Jense, 1996: p116); * = the values are offset and gain respectively; the bold DN values represents DN haze. Note that atmospheric correction can be performed on images that have already been converted into radiance by choosing the offset/gain option and entering an offset of 0 and a gain of 1 (Idrisi Taiga, help).

Geometric correction

All the five satellite images used for this study including the Landsat image series and the ASTER image have been geo-referenced upon acquisition to UTM Zone 32 North, WGS-84 datum. However, geometric corrections were made to adjust distortions in the images for optimum positional accuracy. This is because when comparing two or more images that were collected at different times or from different sources, changes over time can be accomplished by examining the differences in the values of the corresponding cells in multiple images (Eastman, *et al.,* 2007). This process only makes sense, however, if the corresponding pixels of each image actually describe the same location on the ground.

Prior to geometric correction, the two granules of ASTER images for 2005 that covered the study area were mosaicked using "georeference based mosaicking techniques" with a feathering of 10 pixels as implemented in ENVI 5.3 software. The resulting image is henceforth referred to as the reference image (Figure 2). Was rectified using 18 ground control points (GCPs) collected interactively on an already rectified SPOT 5 satellite image of 4/05/2005 obtained from the National Space Research and Development Agency (NASRDA), Abuja

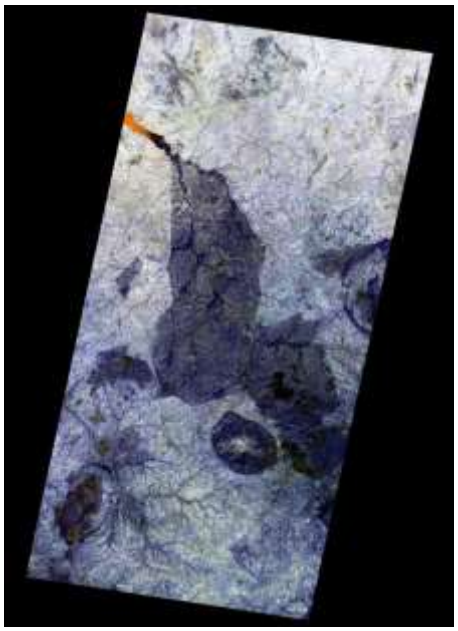

Fig. 2: Mosaicked ASTER image of Falgore Game Reserve in false colour composite

The process yielded a root mean square error (RMSE) of 0.00197 after deleting 10 GCPs indicating that the image was less than one meter error (Table 3). This is within the acceptable range according to Jensen (2005).). These were then used in rectifying the ASTER image using 1st order polynomial transformation method and nearest neighbour resampling algorithm for intensity interpolation of the brightness values (BV) with a UTM projection and 15 x15m pixel.

Table 3: Characteristics of 8 ground control points used to rectify the ASTER 2005 scene

Point Number	Base X	Base Y	Warp X	Warp Y	Predicted X	Predicted Y	Error X	Error Y	RMS
1	2539.46	6224.31	183.60	3530.80	183.60 3	3530.80	0.00	0.00	0.00
2	3186.25	6162.00	1477.25	3404.88	1477.25	3404.88	0.00	0.00	0.00
3	3313.60	5207.20	1734.09	1493.36	1734.09	1493.36	0.00	0.00	0.00
4	2949.40	4728.50	1002.66	535.96	1002.66	535.96	0.00	0.00	0.00
5	2689.00	5524.00	480.93	2128.81	480.93	2128.81	0.00	0.00	0.00
10	2611.50	5281.33	324.78	1643.26	324.78	1643.26	0.00	0.00	0.00
11	2636.50	4854.33	373.72	788.54	373.72	788.54	0.00	0.00	0.00
18	3233.86	5796.71	1573.07	2673.58	1573.07	2673.58	0.00	0.00	0.00

Total RMSerror with the 8 GCPs used in resampling is 0.00197

Finally, an interactive image to image registration was performed to rectify the four Landsat images (1986, 1990, 1998 and 2000) with reference to the 2005 ASTER as the base year image. They were all resampled to 15x15m pixels using nearest neighbor resampling and registered to base image for change detection. It is important to note that the accuracy of geometric rectification can have a direct bearing on the accuracy of a subsequent radiometric normalization. Table 4 presents the summary of the overall RMSE statistics for all the images used, while appendix VI detailed out the geometric rectification process.

Table 4: Characteristics of the remotely sensed satellite data used for exploring changes in vegetation cover in FGR.

Date	Type of Imagery	Nominal instantaneous Field of View (m)	Resampled Pixel resolution	No of GCPs used	Rectification RMSE
19/12/1986	Landsat 5 TM	30 x 30	15 x 15	11	0.496
22/12/1990	Landsat 4 TM	30 x 30	15 x 15	15	0.260
18/11/1998	Landsat 5 TM	30 x 30	15 x 15	12	0.486
17/12/2000	Landsat 7 ETM+	30 x 30	15 x 15	12	0.396
29/11/2005	ASTER	15 x 15	15 x 15	8	0.002

The geographic dynamic link module in ENVI 5.3 was further used to evaluate the accuracy of the geometric correction using 40% transparency dynamic overlay function.

Radiometric normalisation

Using the technique of image normalization (Du, *et al.,* 2002) the four Landsat series were then indirectly normalized for atmospheric absorption with the ASTER image as the reference image. Radiometric normalization of the Images was achieved by applying regression equations to the 1986, 1990, 1998, and 2000 image data set to predict what a given *BV* would be if it had been acquired under the same conditions as the 2005 reference scene. These regression equations were developed by correlating the brightness of PIFs present in both the scene being normalized and the reference (2005) scene (see Figure 3). A total of 3 reservoirs, 2 rock outcrop (the surface of the selected rocky area was smooth and have not vegetation cover) and 2 bare sites were used to normalize the 1986, 1990, 1998 and 2000 data. The 3 PIFs were digitized, rasterized and converted into Boolean images (a value of 1 for the PIFs pixels and 0 for other areas: see Figure 4). The Boolean image was then used as a mask image for regressing all the earlier images against the 2005 ASTER image.

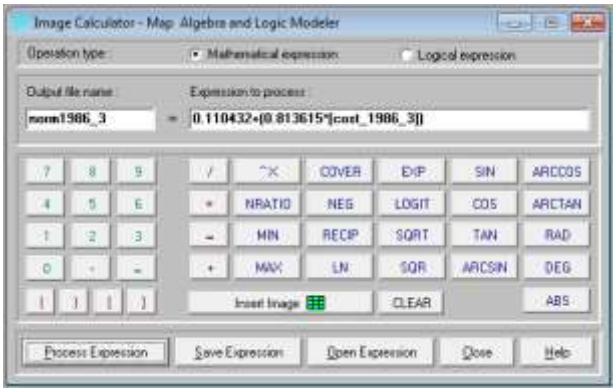

Fig. 3: Implementation of Empirical Regression Scene normalization in Idrisi Using the Image Calculator. This is an example of normalization process for TM1986 band 3 using the coefficients.

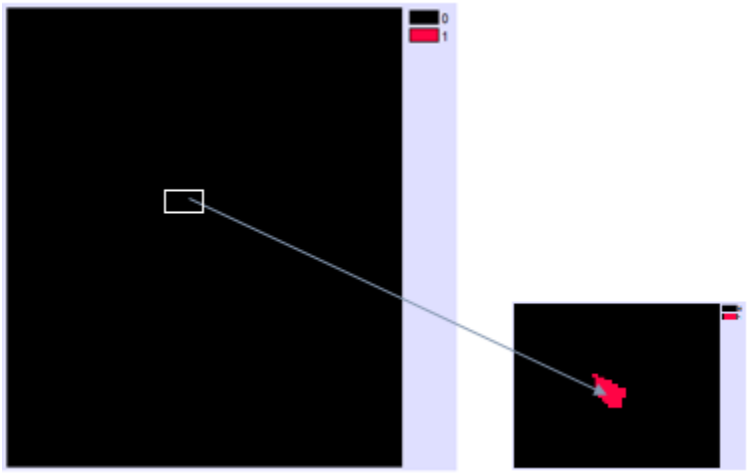

Fig. 4: Boolean Image used as Mask Isolating the PIFs Reflectance Value. Note that the pixels selected were very small in dimension and hence it is difficult to visualize them within the entire image map. The insert to the right is a zoomed section of the image of 10 x 10.

Computing NDVI

The Normalized Difference vegetation Index (NDVI) developed by Rouse *et al.* (1974) which is the ratio of Red and NIR bands was used: .

$$NDVI = \frac{NIR - R}{NIR + R} \quad (3.1)$$

Where *NIR* is the near infra-red band and *R* is the red band.

Image regression change detection

The regression technique accounts for differences in mean and variance between pixel values for different dates and it is assumed that time two is a function of time one. The earlier NDVI was considered as the independent variable and the more recent one was taken to be the dependent variable. A linear relationship was established between these two images. The predicted image and the base image (i.e. time one image) were subtracted from each other after applying the linear regression function.

RESULTS AND DISCUSSIONS

Empirical radiometric normalization using regression coefficient

It is important to note that significant radiometric differences still exist due to residual mismatch of data obtained on different dates by different satellites (Hall *et al.*, 1991; Guo *et al.*, 2008) and the dynamic environmental structure of the study area. As a result of the empirical radiometric normalization procedure employed, the bands 3 and 4 of Landsat products for 1986, 1990, 1998 and 2000 image data were adjusted to a common reference image of bands 2 and 3of ASTER 2005 respectively, using the regression coefficient of the pseudo invariant features (PIFs). The resulting regression models are as shown in Table 5. The reflectance value of the early image targets/PIFs (eg. 1986) were regressed against the reflectance values of the referenced image PIFs (e.g 2005) for band 3 and 4 in the case of Landsat products (1986,1990,1998 and 2000) and bands 2 and 3 for 2005 ASTER product respectively (Figure 5). Only PIFs with a linear coefficient => 0.90 were considered appropriate for the analysis. In this case, the results fulfilled the assumptions and all the models estimated by the regression procedure are significant at an α-level of 0.05, except for the TM_3 1990 which had an r^2 value of 0.10 (Table 5). This showed that the PIFs coefficients are really not good estimators. Because the TM_3 was used for computing NDVI algorithm, it was felt that the error will be shifted to NDVI values for 1990 which could affect the quality of the NDVI product as earlier observed by Kaufmann (1989). Hence, the 1990 image was dropped from further analysis.

Table 5: Image normalization regression models developed for the FGR

Image normalized with the 29 Nov 2005 Aster reference image	Regression models	r^2 (%)
19 Dec 1986 TM	2005ASTER_2 = 0.110432 + 0.813615(TM_3 1986)	90.1
	2005ASTER_3 = 0.09636 + 1.006432(TM_4 1986)	93.2
22 Dec 1990 TM	2005ASTER_2 = -0.052744 + 1.036475(TM_3 1990)	**10.7**
	2005ASTER_3 = 0.049232 + 0.919091(TM_4 1990)	90.0
18 Nov 1998 TM	2005ASTER_2 = 0.100110 + 0.704082(TM_3 1998)	94.1
	2005ASTER_3 = 0.121362 + 0.702687(TM_4 1998)	95.2
17 Dec 2000 ETM+	2005ASTER_2 = 0.087655 + 0.642297(TM_3 2000)	92.7
	2005ASTER_3 = 0.123989 + 0.669437(TM_4 2000)	94.9

a-level of 0.05. Note that the 1990 TM_3 Red band had a very low r^2 value, hence the 1990 dataset was dropped in the analysis.

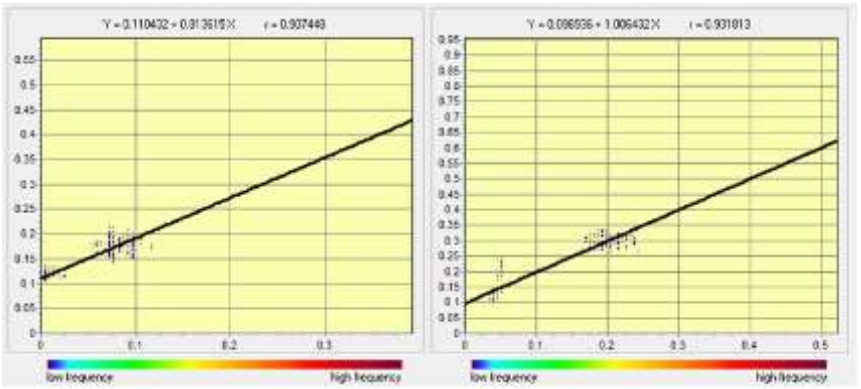

a) 1986 TM_3 (Red) b) 1986 TM_4 (NIR)

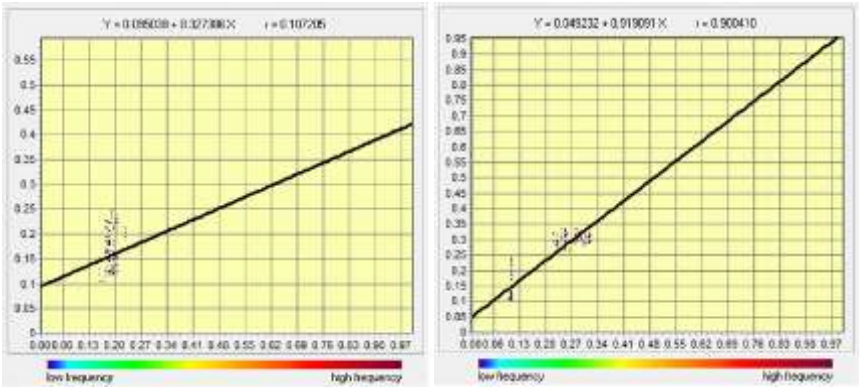

c) 1990 TM_3 (Red) d) 1990 TM_4 (NIR)

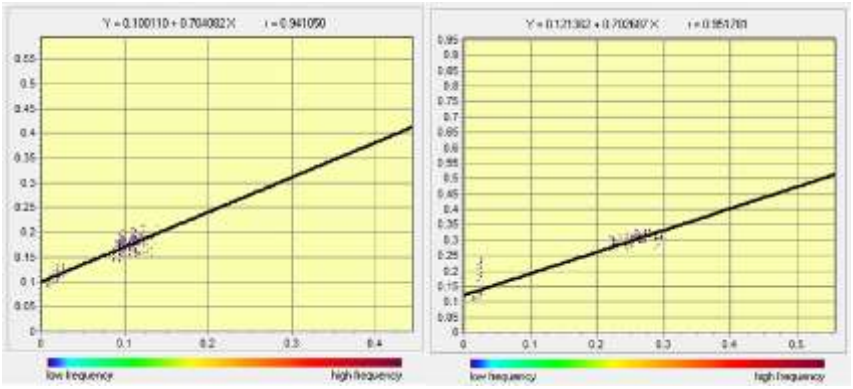

e) 1998 TM_3 (Red) f) 1998 TM_4 (NIR)

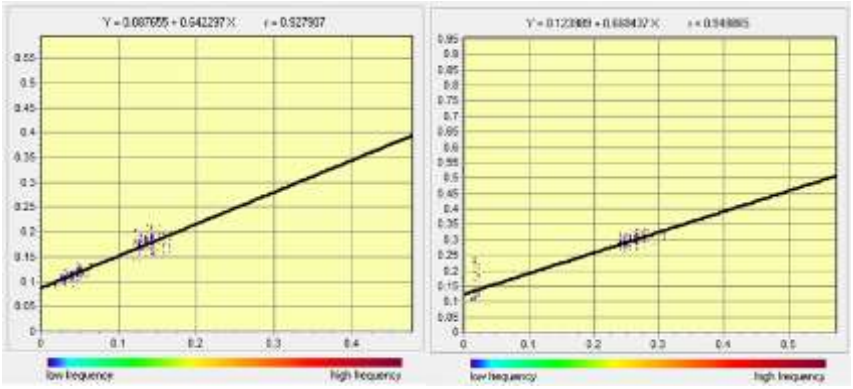

g) 2000 ETM+_3 (Red) h) 2000 ETM+_4 (NIR)

Fig. 5: Linear regression diagram of the different image pairs with PIFs. This shows the relationship between the same PIFs selected (dry and wet areas) found in both images.

The assumption that transformed data that are meant to be corrected for exogenous abnormality usually have their standard deviation reduced. This assertion was examined by comparing the standard deviation of the atmospherically corrected images and the spectrally normalized images (Table 6).

Table 6: Descriptive Statistics of Atmospherically corrected bands

Year	Band	Min	Max	Mean	SD
a) The atmospherically corrected band images after COST-model was applied.					
1986	3	0	0.392	0.085	0.045
	4	0	0.523	0.293	0.076
1990	3	0	1	0.257	0.052
	4	0	1	0.358	0.069
1998	3	0	0.444	0.113	0.044
	4	0	0.558	0.288	0.061
2000	3	0	0.478	0.157	0.053
	4	0	0.573	0.31	0.068
2005	2	0	0.594	0.143	0.107
	3	0	0.956	0.227	0.159

b) The radiometrically normalized images using empirical regression.

1986	3	0.11	0.429	0.180	0.037
	4	0.085	0.524	0.331	0.063
1990	3				
	4				
1998	3	0.1	0.413	0.180	0.031
	4	0.121	0.513	0.324	0.043
2000	3	0.088	0.395	0.189	0.034
	4	0.124	0.507	0.332	0.046
2005	2	0	0.594	0.143	0.107
	3	0	0.956	0.227	0.159

From the descriptive statistics presented in Table 6 it can be observed that there was a reduction in the standard deviations indicating that relative contributions of residual mismatch have reduced greatly. In addition, the result shows that the mean reflectance values have increased and this might not be unconnected with the smoothening effects that had normalized the spikes in the reflectance values (outliers) and removed the additives residual effect of the atmosphere which may have masked some areas thereby increasing those pixel reflectance values. The result is therefore a slight increase in the overall mean reflectance value. This observed pattern testify the fact that the data is fit for onward analysis.

Effect of radiometric normalization on NDVI

The NDVI images were derived using regression models in Table 5 from all the image dates excluding the 1990. Although studies have shown that ratio imagery (NDVI inclusive) especially those produce using Landsat 7 ETM+ data are of excellent quality (Vogelmann*et al.*, 2001). It is important to examine the quality of the NDVI images generated for radiometric normalization as compared to non-normalized products.

The effect of empirical normalization on the NDVI images generated for this study was examined by comparison of derived NDVI images from the three different processing levels (i.e derived NDVI from (a) uncorrected raw DN image data, (b) atmospherically corrected image, and (c) radiometrically normalized image). The essence is to examine the influence of atmospheric correction and radiometric normalization on the quality of NDVI data. Table 7 illustrates the summary of the descriptive statistic of NDVI resulting from the three different levels processing. From the generated statistics, it appears that after applying the atmospheric correction the minimum and maximum values were stretched between -1 and 1 which is the extreme values for NDVI. The implication of having 1 as the maximum value is that the vegetation is very dense and perhaps as dense as those found in irrigated agricultural plots or within the tropical rain forest zone as against the guinea savanna vegetation zone where FGR is situated. This indicates that though there was correction on the images but there still exist some residual mismatch on the scenes creating a saturation of the NDVI values in areas that are known to be savanna. Meanwhile, a closer look at Table 7c reveals that there was decrease in the deviation for all the NDVI images after the radiometric normalization.

To appreciate the impact of radiometric normalization a visual display of the NDVI produced by the three different processing levels is presented in Figure 6. Figure 6a, b and c is a visual display of 1986 NDVI for unprocessed (raw DN value), atmospherically corrected and radiometrically corrected dataset respectively. Visual examination of all the three images shows that anomalies observed within the uncorrected raw and atmospherically corrected images were normalized in Figure 6c. For instance, the clear yellow patches observed in the south eastern part of the study area (Figure 6a) and the corresponding dark green colour in same location (Figure 6b) signifies anomalies in the data, and Figure 6c illustrate the corrective effect on same. In addition, the sharpened boundary of the water bodies (the Tiga dam and other minor reservoirs) spectra in Figure 6c as against those in Figure 6a and 6b support the influence of radiometric normalization on images meant for multi-date comparison. Figure 6d, e and f exemplifies the same effect on 1998 ndvi, and 2000 ndvi image illustrated in Figure 6g, h and j. In all the images (1986, 1998 and 2000) the normal Figure 6k is the base image of ASTER derived-NDVI for 2005 before atmospheric correction, while Figure 6l is the same ndvi –derived image after the application of COST atmospheric correction model.

Table 7: Descriptive Statistics of the NDVI images generated

	Year	Min	Max	Mean	SD
a)	***The ndvi images generated from the raw DN values.***				
	1986	-1	0.348	0.078	0.073
	1990	-0.864	1	0.06	0.073
	1998	-1	0.688	0.209	0.131
	2000	-1	0.319	-0.167	0.086
	2005	-1	0.581	0.063	0.081
b)	***The ndvi images generated after applying the COST-model***				
	1986	-1	1	0.574	0.164
	1990				
	1998	-1	1	0.438	0.194
	2000	-1	1	0.328	0.172
	2005	-1	0.671	0.16	0.131
c)	***The ndvi images derived from the normalized band combination***				
	1986	-0.377	0.555	0.293	0.078
	1990				
	1998	-0.265	0.62	0.285	0.081
	2000	-0.255	0.597	0.276	0.066
	2005	-1	0.671	0.16	0.131

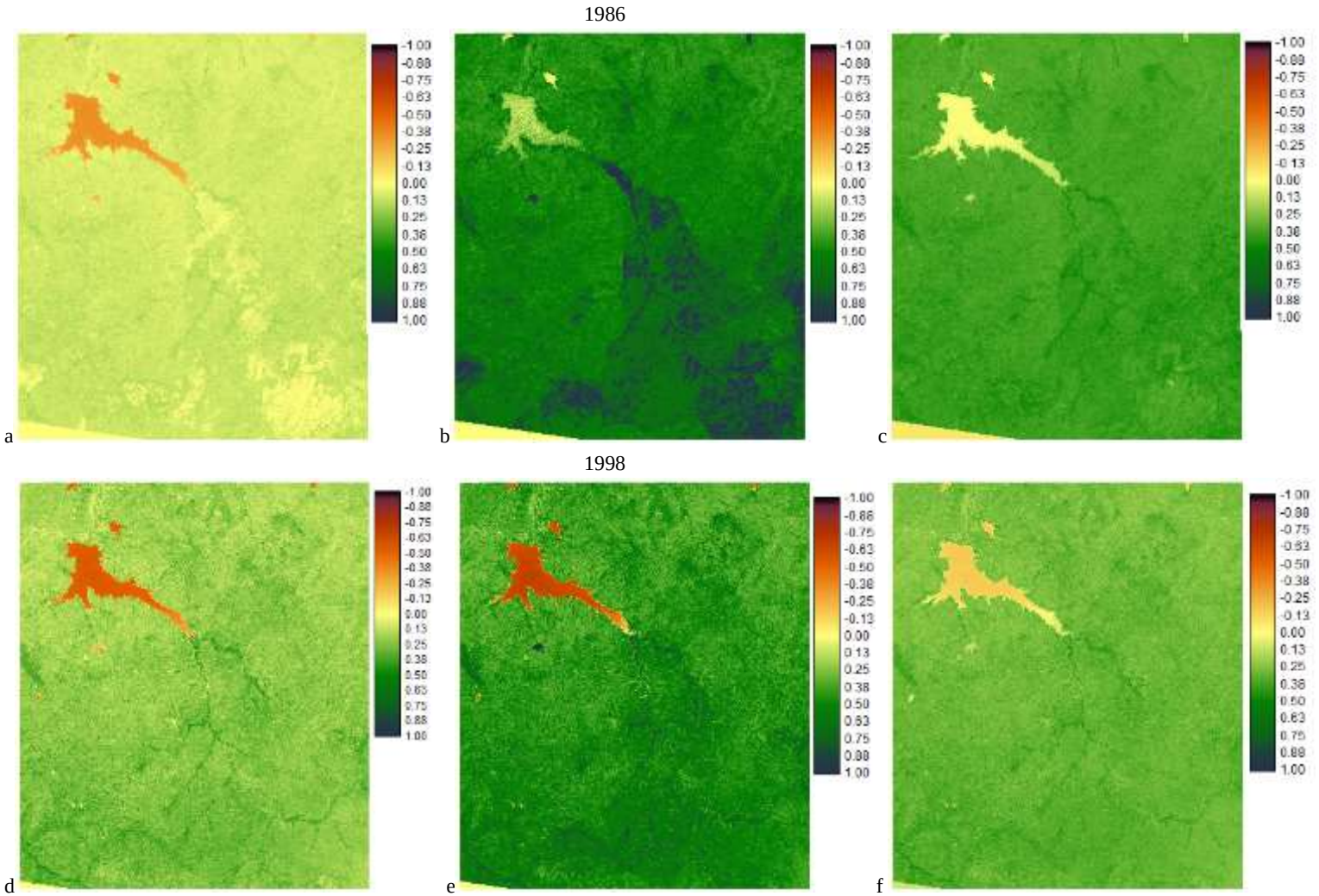

Fig. 6: Effect of radiometric normalization on the NDVI images

[1986 (a) NDVI generated from raw DN values (b) NDVI from atmospherically corrected image (c) radiometrically corrected NDVI]

[1998 (d) NDVI generated from raw DN values (e) NDVI from atmospherically corrected image (f) radiometrically corrected NDVI]

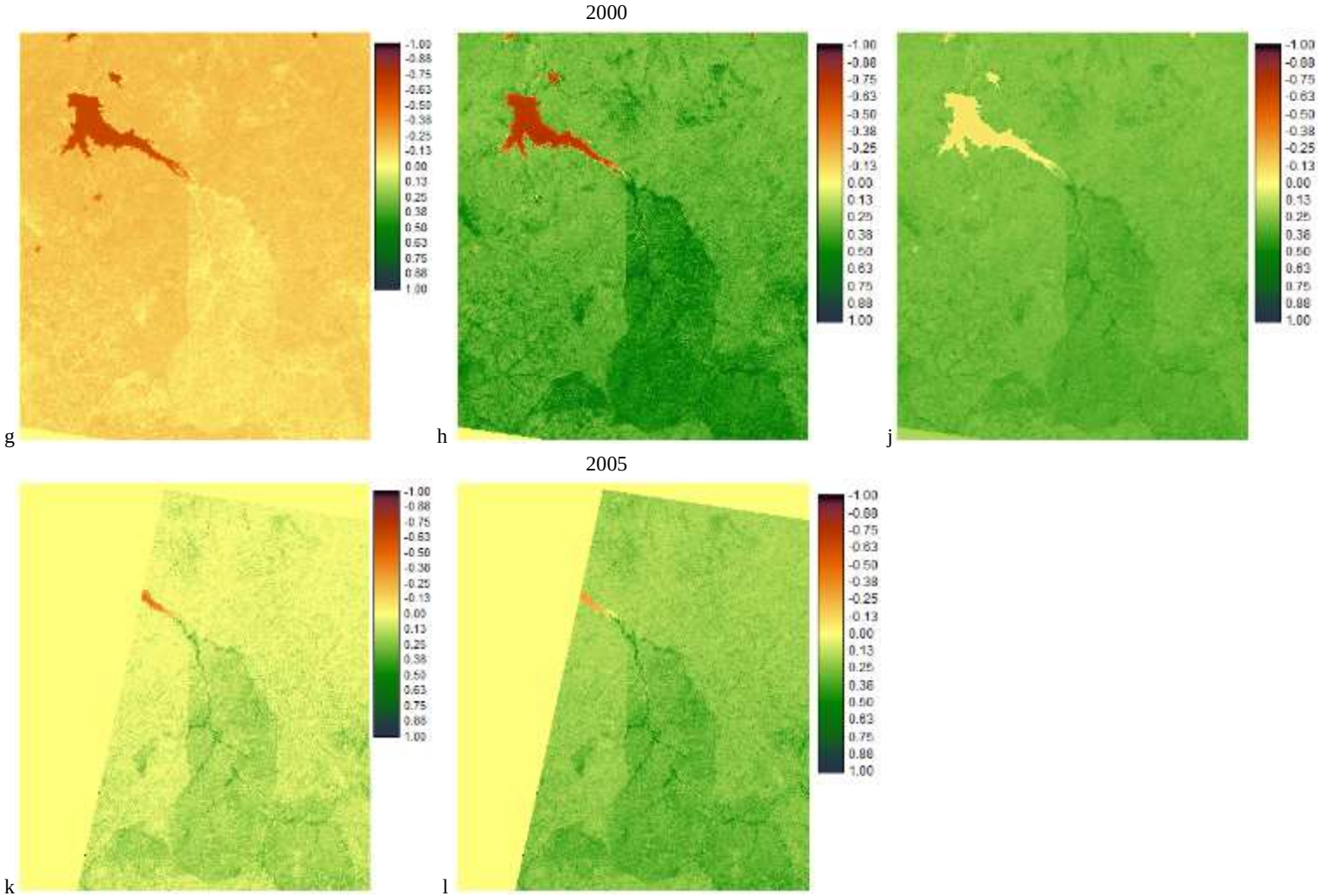

Fig. 6 (Cont.): Effect of radiometric normalization on the images

[2000 (g) NDVI generated from raw DN values (h) NDVI from atmospherically corrected image (j) radiometrically corrected NDVI]

[2005 (k) NDVI generated from raw DN values (l) NDVI from atmospherically corrected image which was then used as base image for correcting the remaining images]

Further verification of the NDVI using histogram plots

The assertion that scene normalization reduces atmospheric attenuations in multi-date comparison images (Munyati, 2000; Jensen, 2005; Berberoglu and Akin, 2009) was further investigated. A subset of the NDVI 1986 image that represents the forested area was used for this purpose (Figure 7). This was done in order to avoid a bimodal histogram plot due to the two main features found within the whole scene i.e water and vegetation. It was therefore felt that the vegetated area will produce a unimodal histogram plot. Figure 8a and b illustrate the histogram of the subset scene of 1986 NDVI before and after radiometric normalization. It can be clear from the two graphs that the effect of spikes in Figure 8a has diminished in 8b and there was a shrink in the spread of the data which is similar to graphs produced during and image enhancement using histogram equalization technique. Table 8 presents a correlation matrix for the three different procedures employed in correcting the image.

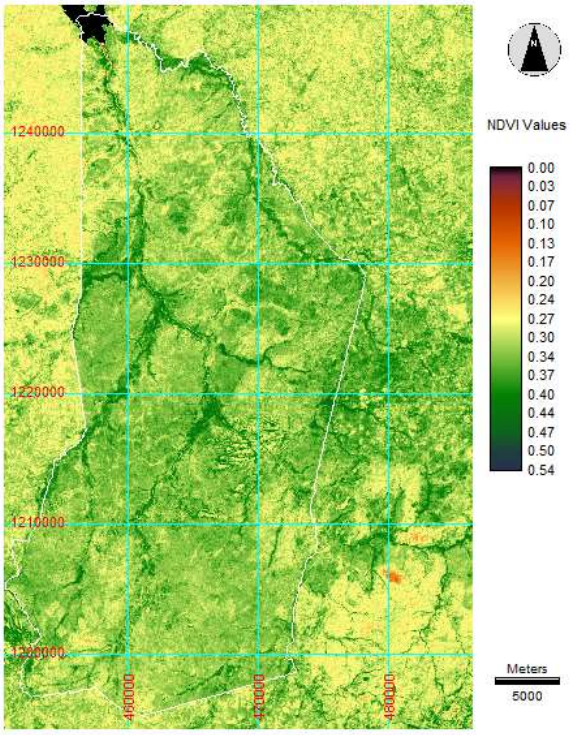

Fig. 7: Windowed Image of the Study area. This subset area was used in the entire analysis.

1986

(a) (b)

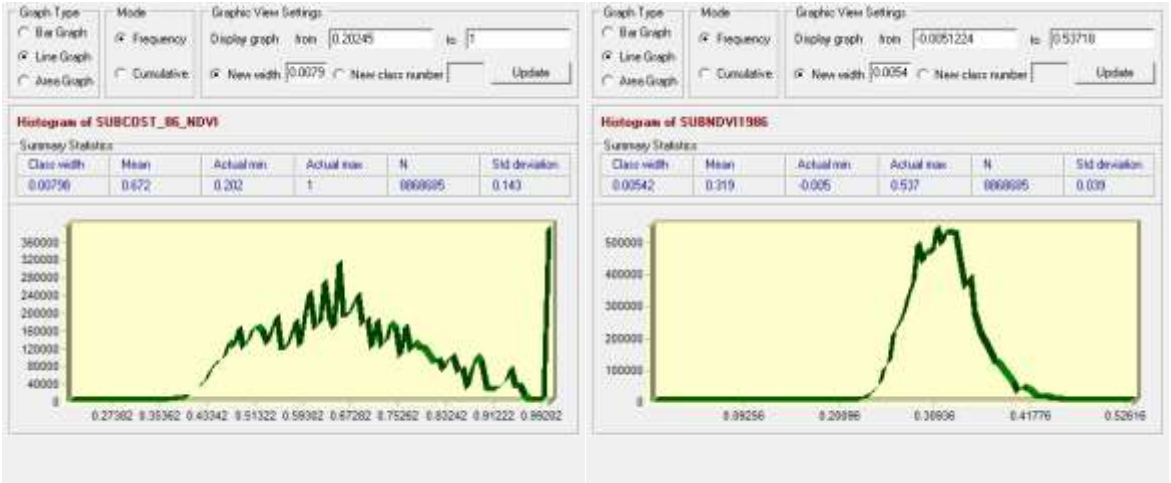

Fig. 8: Histogram plots of NDVI images for the years 1986, 1998, 2000 and 2005 after windowing.

Histogram (a) shows the pattern of NDVI value after conversion of DN values to reflectance values, while (b) shows the pattern of NDVI values of the same image after radiometric normalization with the NDVI values of 2005 as reference image for all the respective years.

Table 8: Correlation matrix for the subset NDVI images

	NDVI Bands			
	1986 NDVI	1998 NDVI	2000 NDVI	2005 NDVI
a) Raw DN images				
1986 NDVI	1.00			
1998 NDVI	0.34	1.00		
2000 NDVI	0.24	0.66	1.00	
2005 NDVI	0.13	0.53	0.74	1.00
b) Atmospherically corrected image				
1986 NDVI	1.00			
1998 NDVI	0.49	1.00		
2000 NDVI	0.64	0.76	1.00	
2005 NDVI	0.57	0.64	0.76	1.00
c) Normalised image				
1986 NDVI	1.00			
1998 NDVI	0.52	1.00		
2000 NDVI	0.55	0.67	1.00	
2005 NDVI	0.40	0.51	0.73	1.00

Note that (a) represent NDVI value for the unprocessed images (raw), (b) NDVI after atmospheric correction, and (c) NDVI after radiometric normalization.

In the last stage, the large water body (edge of the Tiga dam) found around the extreme northwestern part of the windowed image was masked. The descriptive statistics of the output NDVI image is presented in Table 9.

Table 9: Descriptive statistics from the masked windowed NDVI images

Year	Min	Max	Mean	SD
1986	0	0.537	0.318	0.041
1998	-0.089	0.620	0.312	0.045
2000	-0.036	0.597	0.309	0.047
2005	-0.175	0.671	0.266	0.074

Given the above level of data quality control, it is convincing that the normalised NDVI derived data is of higher quality compared with those derived from raw data and atmospherically corrected data alone. And hence, the NDVI data as a new product can be used for further earth process investigation.

CONCLUSION

Radiometric normalization of ASTER data with the Landsat TM and ETM+ using regression of PIFs methods described above produces acceptable results that can be used to examine the NDVI-based spectral variability and surface composition across vegetation woodland. The technique addresses the need to compare multi-date and multi-sensor data acquired for temporal analysis over continues landscape. Although there are challenges to the efficacy of extracting the PIFs, the technique exemplifies a process that seems effective for the woodland terrain. This technique should easily be transferable to other landscapes for effective monitoring especially where NDVI-based change assessment that are associated with saturation owing to poor data handling exist.

REFERENCES

Badamasi, M. M. (2014) Vegetation and Forestry. In A. I. Tanko and S. B. Momale (eds.) *Kano: Environment, Society and Development*. Adonis and Abbey, London: p43-64.

Berberoglu, S. and Akin, A. (2009) Assessing different remote sensing techniques to detect land use/cover changes in the eastern Mediterranean. *International Journal of Applied Earth Observation and Geoinformation*. 11, 46-53.

Brandt, M., Wigneron, J. P., Chave, J., J., Tagesson, T., Penuelas, J., Ciais, P., Rasmussen, K., Tian, F., Mbow, C., Al-Yaari, A., Rodriguez-Fernandez, N., Schurgers, G., Zhang,

W., Chang, J., Kerr, Y. Verger, A., Tucker, C., Mialon, A., Rasmussen, L. V., Fan, L., and Fensholt, R. (2018) Satellite passive microwaves reveal recent climate-induced carbon losses in African drylands. Nature Ecology and Evolution,

Campbell, J. B. (1996) *Introduction to remote sensing*. New York, NY: The Guilford Press

Chavez, P. S. (1988) An improved dark-object subtraction technique for atmospheric scattering correction of multispectral data. *Remote Sensing of Environment*, **24**, 459–479.

Chavez, P. S. (1996) Image-based atmospheric corrections revisited and improved. *Photogrammetric Engineering and Remote Sensing*. 62, (9):1025-1036.

Cracknell, A. P., and Hayes, L. W. B., (1991) *Introduction to Remote Sensing*, London: Taylor and Francis.

Du, Y., Teillet, P. M., and Cihlar, J. (2002) Radiometric normalization of multitemporal high-resolution satellite images with quality control for land cover change detection. *Remote Sensing of Environment*, 82, 123-134

Eastman, J. R., McKendry, J. E. and Fulk, M. A. (2007) *Explorations in Geographic Information Systems Technology, Vol. 1: Change and Time Series Analysis*, Second Edition, United Nations Institute for Training and Research, Geneva. P. 1-51

Eckhartdt, D. W., Verdin, J. P., and Lyford, G. R. (1990) Automated update of an irrigation lands GIS using SPOT HRV imagery. *Photogrammetric Engineering and Remote Sensing*, 56:1515-1522.

Guo, W. Q., Yanga, T. B., Daib, J. G., Shia, L., and Lua, Z. Y. (2008) Vegetation cover changes and their relationship to climate variation in the source region of the Yellow River, China, 1990-2000. *International Journal of Remote Sensing*. 29 (7), 2085-2103.

Hall, F. G., Strebel, D. E., Nickeson, J. E., and Goetz, S. J. (1991) Radiometric rectification: towards a common radiometric response among multidate, multisensory images. *Remote Sensing of the Environment*. 35, 11-27.

Heo, J., and Fitzhugh, T. W. (2000) A standardized radiometric normalization method for change detection using remotely sensed imagery. *Photogrammetric Engineering and Remote Sensing*, 66: 173–181.

Jensen, J. R. (2005) *Introductory Digital Image Processing: A Remote Sensing Perspective*, 3rd edition. Upper Saddle River, New Jersey, Prentice Hall: 526p

Jensen, J. R., Rutchey, K., Koch, M.S. and Narumalani, S. (1995) Inland wetland change detection in the Everglades water conservation area 2A using time series of normalized remotely sensed data. *Photogrammetric Engineering and Remote Sensing*. 61, 199–209.

Kneizys, F. X., Shettle, E. P., Abreu, L. W., Chetwynd, J. H., Anderson, G. P., Gallery, W. O., Selby, J., and Clough, S. A. (1988). User's guide to LOWTRAN 7. Air Force Geophysics Laboratory, Hanscom AFB Environmental Research Report ERP No.1010.

Kottek, M., Grieser, J., Beck, C., Rudolf, B., and Rubel, F. (2006) World Map of the Köppen-Geiger climate classification updated. *Meteorologische Zeitschrift*, 15 (3): 259-263.

Lambin, E.F. (1996) Change detection and multitemporal scales: seasonal and annual variations in landscape variables. *Photogrammetric Engineering and Remote Sensing*. 62, 931–938.

Liman, M., Idris, H. A., and Mohammed, U. (2014) Weather and Climate, In Tanko A. I. and Momale, S. B.(ed.) *Kano: Environment, Society and Development*. Adonis & Abbey, London. 13-20p

McGovern, E. A., Holden, N. M., Ward, S. M. and Collins, J. F. (2002) The radiometric normalization of multitemporal Thematic Mapper imagery of the midlands of Ireland - a case study. *International Journal of Remote Sensing*, 23 (4): 751-766.

Milich, L. and Weiss, E. (2000) GACNDVIInterannualcoeffiecient of variation (CoV) images: ground truth sampling of the Sahel along north-south transects. *International Journal of Remote Sensing*, 21: 235-260.

Munyati, C. (2000) Wetland Change Detection on the Kafue Flats, Zambia, by Classification of a Multitemporal Remote Sensing Image Dataset, *International Journal of Remote Sensing*, 21 (9):1787-1806.

Paolini, L., Grings, F., Sobrino, J.A., Muñoz, J.C.J., Karszenbaum, H., Paolini, L., Grings, F., Sobrino, J.A., Jiménez, J.C. (2006). Radiometric correction effects in Landsat multi- date/multi-sensor change detection studies. *International Journal of Remote Sensing*. 27, 685–704.

Prakash, A. and Gupta, R. P. (1998) Land-use mapping and change detection in a coal mining area- a case study in the Jharia Coalfield, India. *International Journal of Remote Sensing*. 19: 391-410.

Rouse, J. W., Haas, R. H., Schell, J. A. and Deering, D. W. (1974) Monitoring Vegetation Systems in the Great Plains with ERTS, *Proceedings*. Third Earth Resource Technology Satellite 1 Symposium, Green-Belt: NASA SP- 351: 3010-317.

Rustamov, R.B., Salahova, S.E., Zeynalova, M.H., Hasanova, S.N., 2012. Earth Observation-Space Technology.

Schott, J., Salvaggio, C., and Volchok, W. (1998) Radiometric scene normalization using pseudo invariant features. *Remote Sensing of Environment*, 26:1-16.

Syariz, M. A., Lin, B. Y., Denaro, L. G., Jaelani, L. M., Nguyena,M. V., and Lin, C. H. (2019) Spectral-consistent relative radiometric normalization for multitemporal Landsat 8 imagery, ISPRS Journal of Photogrammetry and Remote Sensing, 147: 56–64

Thekaekara, M. P., Kruger, R., and Duncan, C.H., (1969) "Solar Irradiance Measurements from a Research Aircraft", *Applied Optics*, 8 (8):1713-1732.

Turker, C. J., Newcomb, W. W., Los, S. O. and Prince, S. D. (1991) Mean and Inter Year Variation of growing-season Normalised Difference Vegetation Index for the Sahel 1981 - 1989. *International Journal of Remote Sensing*, 12: 1133-1155

Vincent, R. K. (1972) An ERTS Multispectral Scanner experiment for mapping iron compounds, In *Proceedings of the Eight International Symposium on Remote Sensing of Environment*, Ann Arbor, MI (Ann Arbor, MI: Environmental Research Institute of Michigan), pp. 1239–1247.

Vogelmann, J. E., Helder, D, Morfitt, R., Choate, M. J., Merchant, J. W., and Bulley, Henry. (2001) Effects of Landsat 5 Thematic Mapper and Landsat 7 Enhanced Thematic Mapper Plus radiometric and geometric calibrations and corrections on landscape characterization. *Remote Sensing of the Environment*. 78, 55-70.

Wessels, K.J., Prince, S.D., Malherbe, J., Small, J., Frost, P.E. and Vanzyl, D. (2007) Can human-induced land degradation be distinguished from the effects of rainfall variability? A case study in South Africa. *Journal of Arid Environments*, 68, 271–297.

Yelwa, S. A. (2005) Land Cover Changes across Nigeria as Detected from high Temporal Resolution Meteorological Data, *Maiduguri Journal of Arts and Social Science*, 3 (2): 73-79.

Yelwa, S. A. (2008) *Broad scale Vegetation Change Assessment across Nigeria from Coarse Spatial and High Temporal Resolution, A VHRR Data*, Gottingen, Germany: CuvillierVerlag. p350.

Zhang, L., Wu, C., Du, B., 2014. Automatic radiometric normalization for multitemporal remote sensing imagery with iterative slow feature analysis. *IEEE Transaction on Geoscience and Remote Sensing*. 52, 6141–6155.

Zhou, H., Liu, S., He, J., Wen, Q., Song, L., Ma, Y., (2016). A new model for the automatic relative radiometric normalization of multiple images with pseudo-invariant features. *International Journal of Remote Sensing*. 37 (19), 4554–4573.